Evidence of 3D strain gradients associated with tin whisker growth

Johan Hektor[a,*], Jean-Baptiste Marijon[b], Matti Ristinmaa[a], Stephen A. Hall[a], Håkan Hallberg[a], Srinivasan Iyengar[c], Jean-Sébastien Micha[d,e], Odile Robach[d,f], Fanny Grennerat[g], Olivier Castelnau[b]

[a] *Division of Solid Mechanics, Lund University, Box 118, Lund 221 00, Sweden*
[b] *Laboratory PiMM, UMR CNRS 8006, Arts & Métiers ParisTech – CNAM, Paris, France*
[c] *Division of Materials Engineering, Lund University, Box 118, Lund 221 00, Sweden*
[d] *CEA-CNRS CRG-IF BM32 Beamline at ESRF, Grenoble, France*
[e] *Université Grenoble Alpes, INAC-SPrAM and CNRS, SPrAM and CEA, INAC-SPrAM, PCI, Grenoble, France*
[f] *Université Grenoble Alpes, INAC-SP2M and CEA, INAC-SP2M, NRS, Grenoble, France*
[g] *LGT Argouges, Éducation Nationale, Grenoble, France*

A B S T R A C T

We have used Differential Aperture X-ray Microscopy (DAXM) to measure grain orientations and deviatoric elastic strains in 3D around a tin whisker. The results show strain gradients through the depth of the tin coating, revealing a higher strain deeper in the Sn layer. These higher strains are explained by the volume change occurring during growth of the intermetallic phase Cu_6Sn_5 at the interface between the Cu substrate and the Sn coating and at grain boundaries between Sn grains.

Keywords:
Whiskers
Intermetallic compounds
Lead-free solder
X-ray diffraction

Tin whiskers are filamentary tin grains, only a few micrometers wide, but capable of growing to several millimeters in length. Whiskers grow spontaneously from tin coated surfaces and are electrically conducting. This may cause issues due to short-circuiting between components of electronic devices. A number of failures of electronic products due to short circuiting caused by whisker growth have been reported [1]. Until recently, the problem of whisker growth was effectively solved by using Pb–Sn alloys rather than pure Sn. However, due to environmental concerns this solution is no longer available. The ban on the use of lead in electronic devices and components, combined with the current trend of miniaturization, can be envisaged to increase the problems caused by whisker growth in the near future.

Tin whiskers have been an active area of research for over 60 years [2]. Despite this, several questions remain to be resolved regarding the mechanisms causing the whiskers to form and grow. The main hypothesis is that whiskers grow to relax stresses in the tin layer [2–5]. In the case of tin coatings on copper substrates, which is the system studied in this work, the stress is often associated with the volume change caused by the formation and growth of the intermetallic phase Cu_6Sn_5. It has been shown both experimentally [6–9] and by numerical simulations [10,11] that the growth of Cu_6Sn_5 at the interface between the Sn layer and the Cu substrate and at grain boundaries between Sn grains generates compressive stress in the tin layer. However, formation of intermetallic phases is not a necessary condition for whisker growth. Williams et al. [12] report whisker growth on Sn–W samples not forming intermetallic phases. Sobiech et al. [13,14] and Sun et al. [15] claim that the state of stress (tensile or compressive) is unimportant for whisker growth. Instead, they argue that whisker growth is driven by negative strain gradients in the tin layer, i.e. that the strain at the root of the whisker should be more tensile/less compressive than in the surrounding microstructure.

Previous X-ray diffraction studies of tin whiskers have used techniques that only provide spatial resolution in the two dimensions parallel to the Sn coating [4,14,16-18]. This means that the results are averaged over the penetration depth of the X-rays, which is typically on the order of 10 μm. By using Differential Aperture X-ray Microscopy (DAXM) [19–21] diffraction patterns from different depths in a sample can be reconstructed, thus obtaining spatial resolution in three dimensions. This makes it possible to study the grain structure and the strain field around whiskers in greater detail.

* Corresponding author.
E-mail address: johan.hektor@solid.lth.se (J. Hektor).

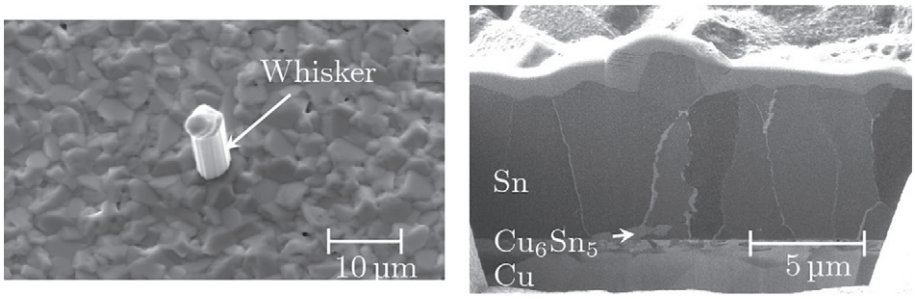

Fig. 1. Left: SEM image of the tin whisker selected for the microdiffraction measurements. Right: FIB cross section showing the columnar grain structure of the Sn layer and the formation of Cu_6Sn_5 at the Cu–Sn interface and at grain boundaries between Sn grains.

In the present work, tin coatings with a thickness of approximately 6.5 µm were deposited on polished 1 mm thick Cu sheets by means of electron beam evaporation. The microstructure of the Sn layer consists of columnar grains, typical for Sn coatings [7,22,23], see Fig. 1. After deposition, the samples were left to age for four months under ambient conditions during which whisker formation took place. Prior to the X-ray experiment, a suitable whisker was located using a scanning electron microscope, see Fig. 1.

The X-ray measurements were performed using the Laue microdiffraction setup on the CRG-IF BM32 beamline at the European Synchrotron Radiation Facility (ESRF) [24]. A polychromatic X-ray beam of 5–23 keV was focused to a spot of 0.7 µm size on the sample using a pair of Kirkpatrick-Baez (KB) mirrors. The sample was mounted at an angle of 40° with respect to the incoming beam and the diffracted X-rays were measured by a Mar CCD 2D detector comprising 2048 × 2048 pixels with a pixel size of about 80 µm, placed at an angle of 90° with respect to the incident beam. This geometry allowed for measurements of reflections in the range $41^\circ \leq 2\theta \leq 139^\circ$.

Conventional Laue microdiffraction can provide information about the crystal structure, orientation, and deviatoric elastic strains of a sample. Due to the penetration depth of the X-rays, the measurements are averaged over the volume probed by the beam [18]. Furthermore, strain determination is less accurate for grains below the surface of the sample. To remedy these limitations, a wire acting as a 'differential-aperture' can be placed between the sample and the detector [19], the experimental setup for DAXM measurements is illustrated in Fig. 2. During the measurement the wire is moved in 1 µm steps parallel to the sample surface and a diffraction pattern is measured for each wire position. By comparing the differential intensity of given detector pixels between two successive wire positions, it is possible to determine the scattering contribution as a function of depth along the beam [20]. The resolution in depth is essentially governed by the distances between the wire, the incident beam and the detector, by the number of steps scanned with the wire, the scanning direction, and (an effect neglected here) by the non-zero transmission of the wire edges [21].

The measured diffraction patterns were analyzed using the LaueTools software [25], being developed at the BM32 synchrotron beamline. The depth-resolved diffraction patterns can be indexed to obtain the crystallographic orientation of each of the grains illuminated by the X-rays. For each reciprocal unit cell an orientation matrix describing the orientation of the unit cell is obtained. From the orientation matrix the direct, $(a, b, c, \alpha, \beta, \gamma)$, and reciprocal, $(a^*, b^*, c^*, \alpha^*, \beta^*, \gamma^*)$, lattice parameters of the deformed crystal can be extracted. Following Ice and Pang [26], the elastic strains, in a frame attached to the crystal lattice and assuming small deformations, can be calculated as

$$\boldsymbol{\varepsilon} = \frac{1}{2}\left(\boldsymbol{A}\boldsymbol{A}_0^{-1} + \left(\boldsymbol{A}\boldsymbol{A}_0^{-1}\right)^T\right) - \boldsymbol{I}, \tag{1}$$

with $\boldsymbol{I}$ being the identity matrix and

$$\boldsymbol{A} = \begin{bmatrix} a & b\cos\gamma & c\cos\beta \\ 0 & b\sin\gamma & -c\sin\beta\cos\alpha^* \\ 0 & 0 & c\sin\beta\sin\alpha^* \end{bmatrix}. \tag{2}$$

the matrix $\boldsymbol{A}_0$ in Eq. (1) is constructed as in Eq. (2) but using the lattice parameters of an unstrained crystal. Unstrained Sn has a body-centered tetragonal structure with lattice parameters $a = b = 5.83$ Å, $c = 3.18$ Å and $\alpha = \beta = \gamma = 90^\circ$ [4]. Since each Laue spot is related to a unique family of lattice planes, variation of the angles between Laue spots directly corresponds to the strain of the unit cell. However, due to the polychromatic beam used in the experiment, it is not possible to determine the volume of the unit cell. For this reason only the deviatoric part of the elastic strain tensor can be determined,

$$\boldsymbol{\varepsilon}^{dev} = \boldsymbol{\varepsilon} - \frac{1}{3}\mathrm{tr}(\boldsymbol{\varepsilon})\boldsymbol{I}, \tag{3}$$

where $\mathrm{tr}(\boldsymbol{\varepsilon})$ denotes the trace of the strain tensor. The effective strain, which is an invariant of the strain tensor, is defined by

$$\varepsilon_{eff} = \sqrt{\frac{2}{3}\boldsymbol{\varepsilon}^{dev} : \boldsymbol{\varepsilon}^{dev}}, \tag{4}$$

with : denoting the double contraction operator.

Two orthogonal lines, 8 µm and 16 µm long, intersecting at the whisker root, were scanned at steps of 0.8 µm using DAXM. In Fig. 3, the reconstruction in depth of four diffraction peaks belonging to two different Sn grains is shown. The diffraction patterns were reconstructed with 1 µm resolution in depth. The first two rows of the figure show Laue spots coming from a grain at the surface of the sample, while the lower two rows show spots from a grain beneath the

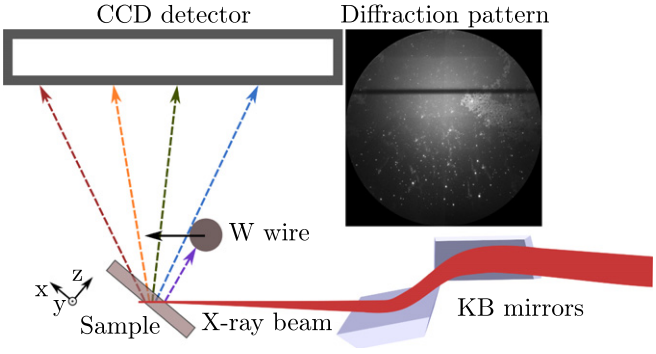

Fig. 2. Schematic view of the experimental setup for Laue microdiffraction. The W wire is only used during the 3D measurements. The wire is seen as a horizontal shadow on the diffraction pattern.

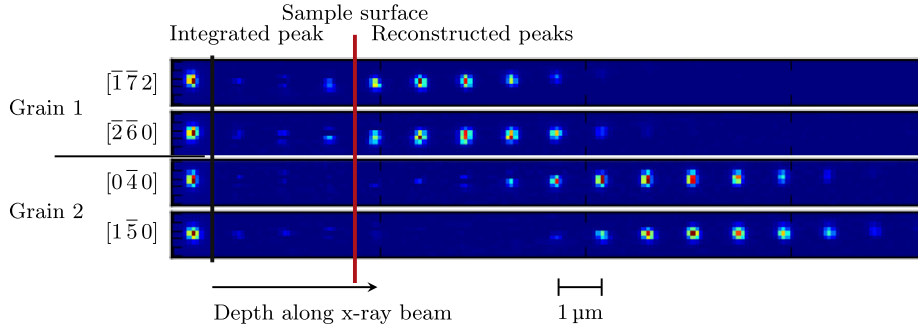

Fig. 3. Laue spots from two different Sn grains, reconstructed in depth along the X-ray beam. The red line indicates the sample surface. To the left the integrated peak is shown, i.e. the peak as measured by the detector when the W wire has been removed. (For interpretation of the references to color in this figure legend, the reader is referred to the web version of this article.)

surface, positioned 5–10 µm below the surface along the incoming beam. Note that due to the 40° tilt of the sample, the depth along the beam is greater than the depth perpendicular to the surface. The slight vertical shift in peak position with increasing depth corresponds to an elongation of the integrated peak and is an indication of strain gradients or rotation within the grains.

In panels b and d in Fig. 4, 2D maps of the grain orientation and effective strain of the Sn grains in a region of 20 × 20 µm around the whisker are shown. The maps were obtained using conventional Laue microdiffraction, i.e. without depth resolution. The grains in the orientation map are color coded based on their Euler angles and it is assumed that the most intense diffraction spots come from the grains on the surface. From the orientation map we see that the grain size is about 3 µm with a few of the grains being elongated in one direction. This is in agreement with the SEM image in Fig. 1. The 2D map of the effective strain shows strain variations across grain boundaries. There are also some grains with strain gradients within the grain. This could be an indication of Cu_6Sn_5 growing at the grain boundaries, thus deforming the region around the grain boundary more than the central part of the grain.

Fig. 4a shows 3D plots of the grain orientations in the Sn coating from the DAXM measurements. It is seen that the DAXM measurements define a columnar grain structure in the tin layer, similar to that obtained by FIB, on a different region of the sample, in Fig. 1. The grain structure is also similar to previous FIB observations published in the literature [27–29]. The whisker grain does not extend all the way through the tin layer, but rather seems to sit on top of another grain. It is also seen that the grain boundaries of the whisker grain are inclined approximately 50° with respect to the surface. This is in good agreement with the growth model proposed by Sarobol et al. [30] in which whiskers form from surface grains with oblique grain boundaries. Note that only a small part of the whisker was scanned using DAXM, as seen in Fig. 4b most of the whisker is located at $x > 0$.

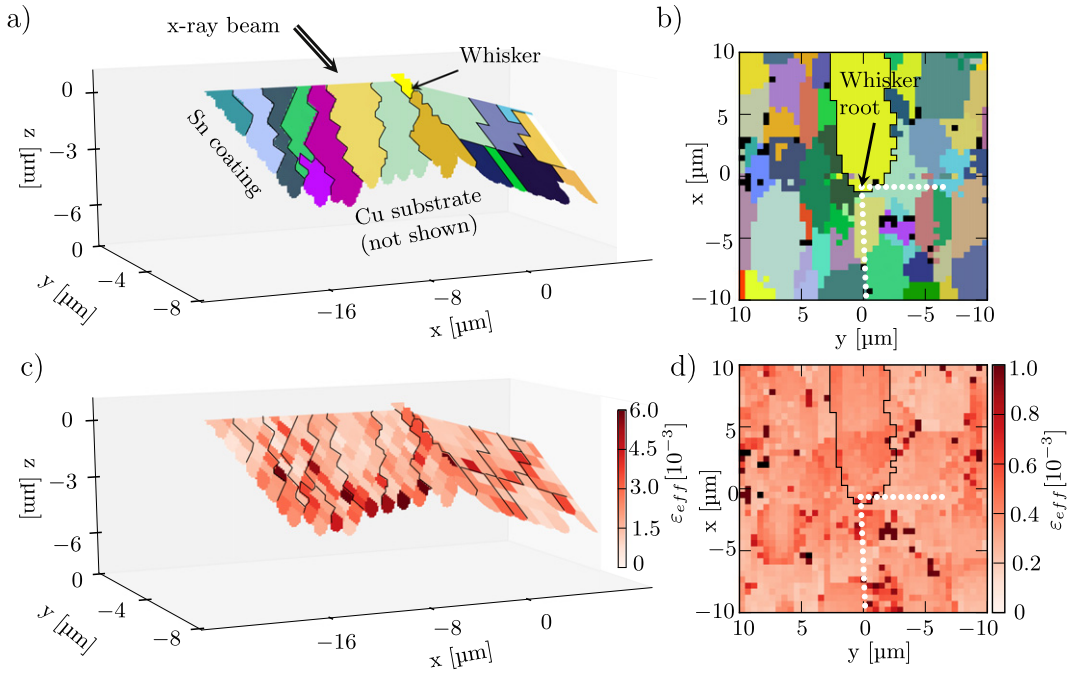

Fig. 4. a): 3D map showing the grain orientations in the Sn coating, obtained from the DAXM measurements. The grains are colored based on their Euler angles. The double lined arrow indicates the direction of the incoming X-ray beam. The coordinates are referring to the coordinate system in Fig. 2, with the origin placed in the whisker root. The surface of the sample is at $z = 0$. b): 2D map of the orientation of the Sn grains around the whisker, obtained by conventional Laue microdiffraction. The black pixels correspond to points where the indexing was not possible. The filled white circles indicate the positions scanned with DAXM. The yellow grain indicated by black lines is the whisker. c): 3D map of the effective strain in the Sn coating. d): 2D map of the effective strain in the region around the whisker. (For interpretation of the references to color in this figure legend, the reader is referred to the web version of this article.)

By comparing the 2D surface map to the 3D map it is possible to identify the same grains in both maps. However, at some positions the 2D map shows a grain which is not located at the surface. For example, the pink grain in Fig. 4a is not found at the correct position in the 2D map in Fig. 4b. This is a consequence of the volume averaging of the diffraction pattern, as grains with a large probed volume will give intense diffraction spots even though they are located below the surface. This indicates that DAXM measurements are necessary even to get a correct representation of the grain structure at the surface. Depth resolution will also increase the credibility of the strain determination.

From the maps of the effective strain in Fig. 4c it is evident that the strain is low at the surface and higher deep in the sample, i.e. there exists a strain gradient in the depth direction. Again, due to the averaging over the probed volume, strain gradients through the depth of the coating can not be seen using conventional Laue microdiffraction. This observation further highlights the need for 3D spatial resolution. The high strain close to the bottom of the tin layer can be explained by the volume change due to formation of the intermetallic compound Cu_6Sn_5, occurring by diffusion of Cu atoms into the Sn layer. Regions of higher strain around some grain boundaries are also present. It is also seen in Fig. 4c that the whisker is not completely strain free, the part of the whisker that is above the sample surface has very low strains, but there is some strain in the root and in the grain below the root. In Fig. 1, Cu_6Sn_5 is forming along grain boundaries between Sn grains, and a Cu_6Sn_5 precipitate is present just below the whisker. Similar formation of Cu_6Sn_5 in the region studied with DAXM could explain the strain in the whisker root and around grain boundaries. High effective strain can also be an indication of plastic deformation. In fact, previous TEM studies of Sn coatings [6,7] reveal dislocation movement from the region close to the intermetallic phase towards the surface of the Sn layer. Furthermore, dislocation pile-ups at the surface can lead to cracking of the surface oxide, which is believed to be a precursor for whisker growth [3,5].

Even though only a single whisker was investigated, the results are consistent with those from other studies and so can be considered to be representative for other whiskers growing from pure tin coatings of similar thickness deposited by e-beam evaporation. The mechanisms behind whisker growth and formation of Cu_6Sn_5 are considered to be the same even for coatings manufactured using other techniques, although additional driving forces, such as additional stress due to plating impurities in the case of electroplating, might be present.

In this work the first successful 3D characterization using DAXM of the grain orientations and deviatoric strain around a tin whisker has been presented. The predicted microstructure, columnar Sn grains with the whisker grain having oblique grain boundaries, corresponds well with FIB studies of a different region on the sample, both in terms of grain shape and grain size. The whisker having angular grain boundaries is also in agreement with theoretical models for whisker formation. Furthermore, the measurements confirm the existence of strain gradients in the depth direction. The strain gradients are believed to be caused by the volume change associated with growth of the intermetallic phase Cu_6Sn_5. The high strain will lead to plastic deformation of the Sn layer and dislocations will pile up at the surface, leading to cracking of the surface oxide. Cracks in the surface oxide are believed to be potential nucleation sites for tin whiskers.

Acknowledgments

The authors would like to thank the company Evatec AG in Trübbach, Switzerland, for sample preparation. The funding provided by the Swedish Research Council (Vetenskapsrådet, VR) under grant nos. 2011-05512 and 2015-05390 is gratefully acknowledged. We are also grateful for the beamtime provided by the ESRF, beamline BM32.

References

[1] D. Bunyan, M.A. Ashworth, G. Wilcox, R.L. Higginson, R. Heath, C. Liu, Trans. Inst. Met. Finish. 91 (2013) 249–259.
[2] G.T. Galyon, IEEE Trans. Electron. Packag. Manuf. 28 (2005) 94–122.
[3] B.-Z. Lee, D. Lee, Acta Mater. 46 (1998) 3701–3714. https://doi.org/10.1016/S1359-6454(98)00045-7.
[4] W. Choi, T. Lee, K. Tu, N. Tamura, R. Celestre, A. MacDowell, Y. Bong, L. Nguyen, Acta Mater. 51 (2003) 6253–6261.
[5] K. Tu, J. Li, Mater. Sci. Eng. A 409 (2005) 131–139.
[6] E. Chason, N. Jadhav, W. Chan, L. Reinbold, K. Kumar, Appl. Phys. Lett. 92 (2008) 171901.
[7] K. Kumar, L. Reinbold, A. Bower, E. Chason, J. Mater. Res. 23 (2008) 2916–2934. https://doi.org/10.1557/JMR.2008.0351.
[8] W. Boettinger, C. Johnson, L. Bendersky, K.-W. Moon, M. Williams, G. Stafford, Acta Mater. 53 (2005) 5033–5050.
[9] G.T. Galyon, L. Palmer, IEEE Trans. Electron. Packag. Manuf. 28 (2005) 17–30.
[10] J. Hektor, M. Ristinmaa, H. Hallberg, S.A. Hall, S. Iyengar, Acta Mater. 108 (2016) 98–109.
[11] E. Buchovecky, N. Jadhav, A.F. Bower, E. Chason, J. Electron. Mater. 38 (2009) 2676–2684.
[12] M. Williams, K.-W. Moon, W. Boettinger, D. Josell, A. Deal, J. Electron. Mater. 36 (2007) 214–219.
[13] M. Sobiech, U. Welzel, E. Mittemeijer, W. Hügel, A. Seekamp, Appl. Phys. Lett. 93 (2008) 011906.
[14] M. Sobiech, M. Wohlschlögel, U. Welzel, E. Mittemeijer, W. Hügel, A. Seekamp, W. Liu, G.E. Ice, Appl. Phys. Lett. 94 (2009) 221901.
[15] Y. Sun, E.N. Hoffman, P.-S. Lam, X. Li, Scr. Mater. 65 (2011) 388–391.
[16] P. Sarobol, W.-H. Chen, A.E. Pedigo, P. Su, J.E. Blendell, C.A. Handwerker, J. Mater. Res. 28 (2013) 747–756.
[17] P. Sarobol, W.-H. Chen, A.E. Pedigo, P. Su, J.E. Blendell, C.A. Handwerker, J. Mater. Res. 28 (2013) 785.
[18] F. Pei, N. Jadhav, E. Buchovecky, A.F. Bower, E. Chason, W. Liu, J.Z. Tischler, G.E. Ice, R. Xu, J. Appl. Phys. 119 (2016) 105302.
[19] B. Larson, W. Yang, G. Ice, J. Budai, J. Tischler, Nature 415 (2002) 887–890.
[20] B.C. Larson, L.E. Levine, J. Appl. Crystallogr. 46 (2013) 153–164.
[21] J.-B. Marijon, (Ph.D. thesis), Ecole Nationale Supérieure d'Arts et Métiers, Paris, France, 2017.
[22] L. Reinbold, N. Jadhav, E. Chason, K.S. Kumar, J. Mater. Res. 24 (2009) 3583–3589. https://doi.org/10.1557/jmr.2009.0431.
[23] M.A. Ashworth, G.D. Wilcox, R.L. Higginson, R.J. Heath, C. Liu, R.J. Mortimer, Microelectron. Reliab. 55 (2015) 180–191. https://doi.org/10.1016/j.microrel.2014.10.005.
[24] O. Ulrich, X. Biquard, P. Bleuet, O. Geaymond, P. Gergaud, J. Micha, O. Robach, F. Rieutord, Rev. Sci. Instrum. 82 (2011) 033908. https://doi.org/10.1063/1.3555068.
[25] J.-S. Micha, LaueTools, Open Source Python Packages for X-ray MicroLaue Diffraction Analysis, 2017, https://sourceforge.net/projects/lauetools/.
[26] G.E. Ice, J.W. Pang, Mater. Charact. 60 (2009) 1191–1201.
[27] G.T. Sheng, C. Hu, W. Choi, K. Tu, Y. Bong, L. Nguyen, J. Appl. Phys. 92 (2002) 64–69.
[28] S.-K. Lin, Y. Yorikado, J. Jiang, K.-S. Kim, K. Suganuma, S.-W. Chen, M. Tsujimoto, I. Yanada, J. Electron. Mater. 36 (2007) 1732–1734.
[29] K. Kim, C. Yu, S. Han, K. Yang, J. Kim, Microelectron. Reliab. 48 (2008) 111–118.
[30] P. Sarobol, J. Blendell, C. Handwerker, Acta Mater. 61 (2013) 1991–2003.